Geochemistry Geophysics Geosystems G3
AN ELECTRONIC JOURNAL OF THE EARTH SCIENCES
Published by AGU and the Geochemical Society

Research Letter
Volume 9, Number 3
6 March 2008
Q03004, doi:10.1029/2007GC001827
ISSN: 1525-2027

Mass-independent fractionation of mercury isotopes in the environment

Sanghamitra Ghosh, Yingfeng Xu, Munir Humayun, and Leroy Odom

Department of Geological Sciences, Florida State University, Tallahassee, Florida, USA (ghosh@magnet.fsu.edu)

National High Magnetic Field Laboratory, Tallahassee, Florida, USA

[1] The toxicity of mercury's methylated species and its biomagnification in aquatic food chains and global dispersion by the atmosphere are the cause of worldwide health problems. Recent reports have observed natural mass-dependent fractionation in mercury isotopes, and recent theoretical work has demonstrated that isotopic separation in mercury is due primarily to nuclear field shifts (nuclear volume effect), and the magnetic spin effect gives rise to mass-independent fractionation (MIF) of odd neutron number isotopes. Now we present analytical evidence of mass-independent isotopic variations in mercury produced by both nuclear volume and magnetic isotope processes. Even mass number isotopes exhibit a pattern indistinguishable from that produced by mass-dependent fractionation, with both positive and negative ^{199}Hg and ^{201}Hg anomalies. MIF is easier to reliably determine in Hg isotopes than mass-dependent fractionation alone, and thus it provides a potentially important key in constraining models of mercury sources and pathways in the environment.

Components: 6314 words, 4 figures, 4 tables.

Keywords: mercury isotope; mass-independent fractionation; nuclear volume effect; magnetic spin effect; environment.

Index Terms: 1041 Geochemistry: Stable isotope geochemistry (0454, 4870).

Received 13 September 2007; **Revised** 16 November 2007; **Accepted** 30 November 2007; **Published** 6 March 2008.

Ghosh, S., Y. Xu, M. Humayun, and L. Odom (2008), Mass-independent fractionation of mercury isotopes in the environment, *Geochem. Geophys. Geosyst.*, *9*, Q03004, doi:10.1029/2007GC001827.

1. Introduction

[2] Mercury is a global-scale pollutant. Although it is well understood that atmospheric deposition plays a cardinal role in the global mercury cycle [*Fitzgerald*, 1995; *Morel et al.*, 1998; *Mason and Sheu*, 2002] and that anthropogenic contributions to the annual atmospheric budget rival those of natural processes, crucial details of the mercury cycle and its fluxes are still uncertain. Mercury has seven stable isotopes (^{196}Hg, ^{198}Hg, ^{199}Hg, ^{200}Hg, ^{201}Hg, ^{202}Hg, ^{204}Hg), with a mass range of >3%, of which six are sufficiently abundant (7–30%) for precise measurement. Attempts at Hg isotope measurement have been limited by its high volatility, high first-ionization potential, and ubiquitous contamination in mass spectrometers, until the recent advent of multicollector inductively coupled plasma–mass spectrometry (MC ICP-MS). With new analytical techniques, variations in the isotopic composition of environmental mercury will become a powerful tool in constraining models of the mercury cycle.

[3] Nearly a century ago, *Bronsted and von Hevesy* [1920] reported that they had achieved a partial

separation of mercury isotopes by evaporation at low pressure. *Nier* [1950] suggested that the inability of researchers to obtain the same values for the isotopic composition of mercury might be due partly to real differences in isotope composition between the mercury reagents used. In recent years, several workers have reported variations in the isotopic composition of mercury of up to −5.5‰ ($\delta^{198}Hg/^{202}Hg$ relative to National Institute of Standards and Technology (NIST) standard reference materials (SRM) 3133) in hydrothermal ore deposits [*Hintelmann and Lu*, 2003; *Smith et al.*, 2005]; −1‰ to +4‰ in sediments [*Foucher and Hintelmann*, 2006]; relative variation of 2‰ in sediment cores [*Jackson et al.*, 2004]. In addition laboratory experiments conducted show a biologically induced −7‰ fractionation in $\delta^{198}Hg/^{202}Hg$ (relative to NIST SRM 3133) during reduction of Hg^{+2} to Hg^0 using a purely cultured bacterium *Escherichia coli* [*Kritee et al.*, 2007]. All these workers reported mass-dependent fractionation for Hg isotopes. Controlling laboratory-induced mass-dependent isotope fractionation in Hg remains a substantial analytical challenge because of the small intrinsic variations of Hg isotope composition (∼1–2‰). While this manuscript was in review, *Bergquist and Blum* [2007] published an important paper that presented measurements of mercury isotopes in samples of fish muscles from different locations and of aqueous solutions of Hg^{+2} from which elemental mercury had been removed experimentally by photoreduction. The fish samples and residual solutions exhibited effects of MIF with ^{199}Hg and ^{201}Hg isotopes being enriched relative to the even A isotopes. *Bergquist and Blum* [2007] suggested that the mechanism for such MIF enrichment (up to 2.5‰ in the photoreduction experiments and 4‰ in fish) is the magnetic isotope effect.

[4] Recently, *Schauble* [2007] has made estimations of equilibrium $^{198}Hg/^{202}Hg$ separation factors for a number of mercury species relative to Hg^0 vapor. He showed that the nuclear field shift (due to changes in nuclear volume) is far more significant than zero-point energy differences (vibrational frequency) in effecting isotopic separation. Although, nuclear radii are to first approximation a simple function of mass, in detail the nuclei of odd isotopes exhibit a smaller $\Delta r/A$ than the nuclei of the even isotopes so that the nuclear field shift deviates from mass-dependent isotope fractionation [*Schauble*, 2007]. For mercury isotopes, *Buchachenko et al.* [2004, 2007] demonstrated a mass-independent magnetic isotope effect in the thermal reaction between creatine kinase with methylmercury chloride (CH_3HgCl) and photochemical decomposition of an organomercury compound. Such effects are expressed in the odd A Hg isotopes (^{199}Hg: −1/2, ^{201}Hg: −3/2), because of their nonzero nuclear spin, relative to the even A Hg isotopes (^{198}Hg, ^{200}Hg, ^{202}Hg, ^{204}Hg). We present analyses of Hg isotope composition of environmental Hg by MC-ICP-MS corrected for mass-dependent fractionation. We refined the calculations of nuclear field shift [*Schauble*, 2007] for the Hg isotopes using the most precise published nuclear radii available, and employ the slope of the correlation between ratios of $^{199}Hg/^{202}Hg$ and $^{201}Hg/^{202}Hg$ to establish what fraction of the mass-independent effect is related to nuclear field shift. The difference is assigned to nuclear spin effects.

2. Materials and Methods

[5] Samples from two peat cores, sediment and soil standards for Hg elemental abundances, and Spanish mosses, were analyzed for Hg isotope composition. A peat core representing about 2000 years of accumulation from an ombrotrophic peat bog of Penido Vello, Spain, previously identified as having an anthropogenic Hg profile [*Martínez-Cortizas et al.*, 1999], was serially sampled for Hg isotope analysis. The core was collected jointly by researchers from University of Santiago de Compostela and National High Magnetic Field Laboratory (NHMFL), Florida State University, adjacent to the core previously reported by *Martínez-Cortizas et al.* [1999]. The peat was sampled by cutting cores of 25 × 25 × 25 cm with a serrated stainless steel knife, to a depth of 100 cm. The fresh core was then sliced into 2 cm slices and wrapped in plastic bags and shipped to the NHMFL laboratory. The samples were kept frozen until use. A peat sample from Patagonia was obtained from Harold Beister from University of Heidelberg. Spanish moss samples were collected in Tallahassee, Florida. The sediment and soil are NIST Standard Reference Materials Estuarine Sediment 1646 a and Montana I Soil 2710, respectively.

[6] The ombrotrophic Penido Vello peat core in this study represents ∼2000 years of atmospheric mercury deposition. Ombrotrophic bogs have always been assumed to represent reliable historical mercury repositories based on their spatial homogeneity and absence of mercury migration after deposition [*Benoit et al.*, 1994; *Grigal*, 2003]. Mercury is known to be immobile when bound to

Table 1. Configuration of the Faraday Collectors for Mercury Isotope Ratio Measurements

Measurement	Hg and Pb
L4	...
L3	...
L2	198
L1	199
C	200
H1	201
H2	202
H3	204
H4	206

soil organic matter largely because of the affinity of Hg^{+2} to sulfur-containing functional groups in humic substances [*Schuster*, 1991; *Xia et al.*, 1999; *Yin et al.*, 1997]. Hg^{+2} is also known to go into dissolved phase by getting absorbed onto soluble organics such as fulvic acids [*Lindqvist et al.*, 1991; *Meili*, 1991; *Mierle and Ingram*, 1991]. However, the amount of mercury that gets into a dissolved phase is considered to be a very small fraction of the amount of mercury that is bound to organic matter and stored in bogs [*Biester et al.*, 2002]. On the other hand a recent report by *Biester et al.* [2003] demonstrated that concentrations and accumulation rates of mercury in peatlands are strongly influenced by biochemical alteration of the peat during humification. Owing to mercury's strong affinity toward humic substances, the concentrations of mercury in peat increase as a result of mass losses during humification and the variations in mercury concentrations in peat cores do not necessarily reflect the variations in external mercury fluxes to the bog [*Biester et al.*, 2003].

[7] For sample preparation it is very important to recover mercury from the sample without introducing isotopic fractionation during sample chemistry. A cold acid leaching technique has proved to be excellent for high recovery of mercury in Standard Reference Materials NIST 2704 Buffalo River Sediment and NIST 1572 Citrus Leaves (98% to 100% yield). The same technique was applied to all samples for the current study. The leaching was done at room temperature. A mixture of ultrapure concentrated HCl and 30% H_2O_2 (45 mL, 2:1 v/v) was added to sample in a tightly capped 120 mL PFA vessel (Savillex). The samples were shaken for an hour on a C1 platform Shaker (New Brunswick Scientific Classic Series). The samples were then ultrasonicated for 48 h in an ultrasonic bath of high-purity water. The leachate was then filtered from the residual sample by passing through a 0.2 um Millipore polycarbonate membrane filter in a vacuum filtration system. The quantity of sample leached varied from 1–30 g depending on the concentration of mercury and was adjusted to yield a final concentration of approximately 1 ng/mL of mercury. The total procedural blank including cold acid leaching of sample and vacuum filtration were below 30 ρg.

[8] The 1 ppb (1 ng/mL) mercury standard solutions were prepared fresh daily by dilution of the NIST SRM3133 mercury standard. A 2% tin chloride solution ($SnCl_2$, 98% purity, ACROS) was prepared in 1M HCl daily. The solution was purged every day prior to use with argon gas for approximately 30 min in order to release any trace mercury present. Reagents used in this work included in-house doubly distilled HNO_3 and HCl acids stored in PFA Teflon vessels, analytical grade H_2O_2 (30% Certified ACS, Fisher Chemical), and 18 MΩ QD H_2O.

[9] Mercury isotopic measurements were performed on a Thermo-Finnigan Neptune MC-ICP-MS equipped with eight movable Faraday cups and a fixed Axial Faraday collector. Elemental Hg vapor, formed by reacting sample solution with 2% $SnCl_2$, was introduced into the mass spectrometer by a CETAC HGX-200 Hydride Generation and Cold Vapor System [*Klaue and Blum*, 1999]. A Perimax Spectec peristaltic pump was used to control the intake rates of $SnCl_2$ and Hg sample solutions. The peristaltic pump speed was adjusted to 22 rpm which made the solution uptake rate 1.4 mL/min. The mercury vapor generated from the reduction is transferred by Teflon PFA tubes to the plasma. In between samples the hydride generator system was washed with 1M HCl for 2–3 min until the signal intensity returned to background level.

[10] For mercury isotope ratio measurements seven adjustable Faraday cups were used (Table 1). ^{204}Pb isobaric interference on ^{204}Hg was monitored at mass 206 (^{206}Pb). For a typical ^{202}Hg signal intensity of 800 mV, the ^{206}Pb intensity was $<2 \times 10^{-2}$ mV, resulting in a correction of <0.006‰ on δ^{204}Hg, which is negligible. Operating conditions of the mass spectrometer are listed in Table 2. Data were acquired using 1 block of 50 cycles with an integration time of 8 s. A baseline measurement collecting 30 ratios (total time of 90 s) using the defocusing beam technique was performed at the beginning of each measurement. Peak centering was performed at the beginning of each measurement. Raw isotope ratios ^{198}Hg/^{202}Hg, ^{199}Hg/^{202}Hg,

Table 2. Operating Conditions of Neptune Mass Spectrometer and Hydride Generator

	Values
Plasma Tune Parameters	
Cool gas	15.00 L min^{-1}
Auxiliary gas	0.75–0.85 L min^{-1}
Sample gas	0.7–0.9 L min^{-1}
Additional gas	0.23 L min^{-1}
RF Power	1200
Peripump speed	22 rpm
Cetac HGX-200 Hydride Generation and Cold Vapor System	
Solution uptake rate	1.418 mL min^{-1}
Sensitivity for ^{202}Hg vapor	600–700 mV $(ng/mL^{-1})^{-1}$
Background	8–10 mV

^{200}Hg/^{202}Hg, ^{201}Hg/^{202}Hg and ^{204}Hg/^{202}Hg were calculated from signal intensities. Instrumental mass bias was determined to be about 3–4‰ based on replicate analyses of the NIST SRM 3133 solution. In order to minimize effects of instrumental fractionation, isotope ratios were determined by sample-standard bracketing technique and reported in δ (‰) notation relative to NIST SRM 3133 Hg elemental standard,

$$\delta^{A}\mathrm{Hg} = \left[\left(^{A}\mathrm{Hg}/^{202}\mathrm{Hg}\right)_{\mathrm{sample}} / \left(^{A}\mathrm{Hg}/^{202}\mathrm{Hg}\right)_{\mathrm{NIST3133}} - 1\right] \times 1000 \quad (1)$$

Deviations from mass-dependent fractionation were calculated as

$$\Delta^{A}\mathrm{Hg} = \delta^{A}\mathrm{Hg}_{\mathrm{measured}} - \delta^{A}\mathrm{Hg}_{\mathrm{MD}} \quad (2)$$

The value Δ^{199}Hg and Δ^{201}Hg is defined as the difference between the measured δ^{199}Hg and δ^{201}Hg ($\delta^{A}\mathrm{Hg}_{\mathrm{measured}}$) of a sample and the δ^{199}Hg and δ^{201}Hg ($\delta^{A}\mathrm{Hg}_{\mathrm{MD}}$) obtained from the linear scaling defined by the even mass isotopes. Linear and exponential mass bias correction laws yield Δ^{199}Hg and Δ^{201}Hg values within the uncertainty of our analyses (~±0.1‰). In this paper, the linear scaling factors are derived by least squares fitting of the δ values of the even A isotopes.

[11] The internal precision of each measurement was calculated as the 2 SE of the mean of n runs, where n = 50, or multiples of 50 for larger samples, and is shown in Table 3 for each analysis. The long-term analytical reproducibility of mercury isotope measurements is demonstrated by repeated analysis of NIST SRM 3133 Hg standard (Figure 1a). The total number of measurements is 350 during 16 individual measurement sessions over a period of 6 months. From the entire set of raw ^{198}Hg/^{202}Hg ratios calculated directly from run intensities, an average of 0.327931 ± 0.000611 (±2σ, n = 350) is obtained for the NIST SRM 3133 Hg standard. From the Δ^{199}Hg and Δ^{201}Hg values calculated for the NIST SRM 3133 Hg standard and Almaden cinnabar we infer that the external precision of our Hg measurements is better than 0.1‰ (2σ) for both Δ^{199}Hg and Δ^{201}Hg (Figures 1b and 1c). No systematic trend is observed in the distribution of the Δ^{199}Hg and Δ^{201}Hg per mil values of the NIST and cinnabar (Figures 1b and 1c). This precision can be compared with the reproducibility of the four replicates run on samples which involved both the chemical separation and mass spectrometry, which is always better than 0.1‰ (Table 3). Since mercury is introduced to the plasma in the elemental vapor form (Hg^0), no matrix effects are expected.

3. Results and Discussion

[12] Figure 2 shows two features that consistently exist in our data for all samples analyzed. The δ values for even A isotopes are closely proportional to mass number. A second feature of the data is the mass-independent fractionation of odd mass number isotopes ^{199}Hg and ^{201}Hg. Table 3 gives the Δ^{199}Hg and Δ^{201}Hg values for the samples. Such odd mass number isotopic excursions from the even A array (odd-even staggering) are characteristic of the nuclear field effect on atomic spectra and atomic and molecular electron structure [*Bigeleisen*, 1996; *Gerstenkorn and Verges*, 1975].

[13] The mass-independent fractionation resulting from the nuclear volume effect for a pair of Hg isotopes (^{i}Hg/^{202}Hg) is given with respect to the fractionation in ^{198}Hg/^{202}Hg by:

$$\Delta^{i}Hg = \delta^{198}Hg\left(A^{i}_{NV} - A^{i}_{MD}\right) \quad (3)$$

where A_{NV} is the scale factor for the mass-independent isotope shift, and A_{MD} is the scale factor for the zero-point energy (mass dependent) isotope shift. The scale factor, A_{MD}, is calculated entirely from the masses of the isotopes [*Schauble*, 2007] and the scale factor, A_{NV}, is calculated from the RMS nuclear charge radii of the isotopes [*Schauble*, 2007]. The values of A_{NV} given by *Schauble* [2007] are based on a compilation of nuclear radii [*Angeli*, 2004] and indicate important deviations in ^{199}Hg, ^{201}Hg and ^{204}Hg. However,

Table 3. Δ^{199}Hg and Δ^{201}Hg Values for Natural Samples and Relative Contributions of Magnetic Isotope Effect and Nuclear Volume Effect on Δ^{199}Hg and Δ^{201}Hg[a]

Sample	Δ^{199}Hg	Δ^{201}Hg	Δ^{199}Hg/ Δ^{201}Hg	MIE Contribution		NV Contribution	
				Δ^{199}Hg, %	Δ^{201}Hg, %	Δ^{199}Hg, %	Δ^{201}Hg, %
Patagonia Peat	0.20 ± 0.01	0.10 ± 0.01	2.00	9 ± 5	19 ± 5	91 ± 6	81 ± 5
Patagonia Peat (R)	0.22 ± 0.03	0.12 ± 0.01	1.83	15 ± 4	29 ± 3	85 ± 6	71 ± 6
SRM 2710	0.18 ± 0.04	0.13 ± 0.02	1.38	45	65	55	35
ES 1646	0.15 ± 0.03	0.12 ± 0.03	1.25	57 ± 4	75 ± 4	43 ± 4	25 ± 4
Spanish Moss	−0.83 ± 0.02	−0.98 ± 0.02	0.85	85	93	15	7
Spanish Moss (R)	−0.95 ± 0.02	−1.02 ± 0.02	0.93	96	98	4	2
Almaden Cinnabar	−0.07 ± 0.09	−0.06 ± 0.09	1.40	77 ± 7	89 ± 7	23 ± 7	11 ± 7
Penido Vello Peat							
0–2	−0.32 ± 0.02	−0.42 ± 0.02	0.76	77 ± 2	88 ± 1	23 ± 2	12 ± 1
0–2 (R)	−0.27 ± 0.03	−0.48 ± 0.03	0.56	64 ± 3	81 ± 3	36 ± 3	19 ± 3
2–4	−0.28 ± 0.05	−0.33 ± 0.07	0.85	83 ± 9	92 ± 9	17 ± 9	8 ± 9
4–6[b]	−0.23 ± 0.01	−0.30 ± 0.01	0.77	77 ± 3	89 ± 2	23 ± 3	11 ± 2
6–8	−0.16 ± 0.02	−0.27 ± 0.03	0.59	67 ± 6	82 ± 6	33 ± 6	18 ± 5
10–12	−0.24 ± 0.01	−0.32 ± 0.01	0.75	75 ± 2	87 ± 2	25 ± 2	13 ± 2
12–14	−0.28 ± 0.02	−0.33 ± 0.02	0.85	83 ± 4	92 ± 4	17 ± 3	8 ± 2
14–16[b]	−0.26 ± 0.03	−0.48 ± 0.03	0.54	64 ± 3	80 ± 2	36 ± 3	20 ± 2
16–18	−0.31 ± 0.02	−0.37 ± 0.02	0.84	84 ± 4	92 ± 3	16 ± 4	8 ± 4
20–22[b]	−0.25 ± 0.03	−0.42 ± 0.04	0.60	66 ± 7	81 ± 7	34 ± 5	19 ± 5
22–24	−0.35 ± 0.03	−0.35 ± 0.03	1.00	89 ± 6	95 ± 6	11 ± 6	5 ± 6
26–28[b]	−0.38 ± 0.03	−0.46 ± 0.03	0.83	84 ± 5	92 ± 4	16 ± 5	8 ± 4
30–32	−0.20 ± 0.03	−0.31 ± 0.05	0.65	68 ± 5	83 ± 5	32 ± 5	17 ± 5
32–34	−0.33 ± 0.03	−0.42 ± 0.03	0.79	80 ± 5	90 ± 4	20 ± 5	10 ± 4
34–36	−0.25 ± 0.03	−0.35 ± 0.03	0.71	74 ± 5	87 ± 4	26 ± 5	13 ± 4
38–40	−0.31 ± 0.01	−0.37 ± 0.02	0.84	85 ± 3	93 ± 3	15 ± 3	7 ± 3
42–44	−0.35 ± 0.04	−0.43 ± 0.03	0.81	82 ± 3	91 ± 3	18 ± 3	9 ± 3
44–46	−0.29 ± 0.02	−0.36 ± 0.03	0.81	81 ± 4	91 ± 4	19 ± 4	9 ± 4
46–48[b]	−0.28 ± 0.08	−0.24 ± 0.08	1.17	68 ± 14	83 ± 13	32 ± 14	17 ± 13
50–52	−0.39 ± 0.01	−0.38 ± 0.02	1.03	85 ± 5	93 ± 4	15 ± 5	7 ± 4
54–56	−0.36 ± 0.04	−0.37 ± 0.03	0.97	96 ± 8	98 ± 7	4 ± 8	2 ± 7
56–58	−0.43 ± 0.02	−0.39 ± 0.03	1.10	78 ± 6	89 ± 6	22 ± 6	11 ± 6
58–60	−0.41 ± 0.03	−0.43 ± 0.03	0.95	99 ± 6	100 ± 5	1 ± 5	0 ± 5
62–64	−0.50 ± 0.04	−0.41 ± 0.04	1.22	61 ± 7	78 ± 7	39 ± 7	22 ± 7
64–66	−0.39 ± 0.01	−0.48 ± 0.01	0.81	80 ± 2	90 ± 1	20 ± 2	10 ± 1
66–68	−0.35 ± 0.01	−0.36 ± 0.01	0.97	98 ± 1	99 ± 1	2 ± 1	1 ± 1
70–72	−0.32 ± 0.02	−0.33 ± 0.03	0.97	98 ± 5	99 ± 5	2 ± 5	1 ± 5
74–76	−0.33 ± 0.03	−0.46 ± 0.02	0.72	72 ± 3	86 ± 2	28 ± 3	14 ± 2
78–80	−0.32 ± 0.03	−0.37 ± 0.03	0.86	86 ± 5	93 ± 4	14 ± 5	7 ± 4
82–84	−0.34 ± 0.03	−0.39 ± 0.04	0.87	88 ± 6	94 ± 5	12 ± 6	6 ± 5
84–86	−0.33 ± 0.03	−0.37 ± 0.02	0.89	91 ± 5	96 ± 4	9 ± 5	4 ± 4
86–88	−0.36 ± 0.03	−0.46 ± 0.04	0.78	79 ± 3	89 ± 2	21 ± 3	11 ± 2
90–92	−0.31 ± 0.03	−0.37 ± 0.03	0.84	84 ± 5	92 ± 4	16 ± 5	8 ± 4
90–92 (R)	−0.37 ± 0.02	−0.36 ± 0.02	1.03	88 ± 6	95 ± 3	12 ± 6	5 ± 3
92–94	−0.35 ± 0.02	−0.42 ± 0.02	0.83	86 ± 3	93 ± 3	14 ± 3	7 ± 3
94–96	−0.22 ± 0.03	−0.27 ± 0.04	0.81	82 ± 7	91 ± 6	18 ± 7	9 ± 6
96–98	−0.31 ± 0.02	−0.44 ± 0.02	0.70	73 ± 3	86 ± 2	27 ± 3	14 ± 2

[a] MIE is magnetic isotope effect. Δ^{199}Hg and Δ^{201}Hg values are given in per mil. See text for details on how Δ^{n}Hg per mil has been calculated. The internal precision of each measurement was calculated as the 2 SE of the mean of n runs, where n = 50, or multiples of 50 for larger samples. For Almaden cinnabar, the error represents 2σ on 60 replicates. The sediments are NIST Standard Reference Materials Estuarine Sediment 1646 a and Montana I Soil 2710.

[b] Samples correspond to samples for which replicate runs were not possible because of constraints on available sample mass, and the errors represent internal precision from 50 scans of a single analysis. R represents duplicate replicate runs on samples which involved both the chemical separation and mass spectrometry.

isotope shifts in the Hg arc spectrum [*Gerstenkorn and Verges*, 1975] are linearly correlated with mass number for even A mercury isotopes including ^{204}Hg, as are our measured δ values (Figure 3). We therefore reexamined the values of A_{NV} using the most precise empirically determined values of the nuclear radii, which were determined from muonic X-ray transitions in separated stable Hg isotopes

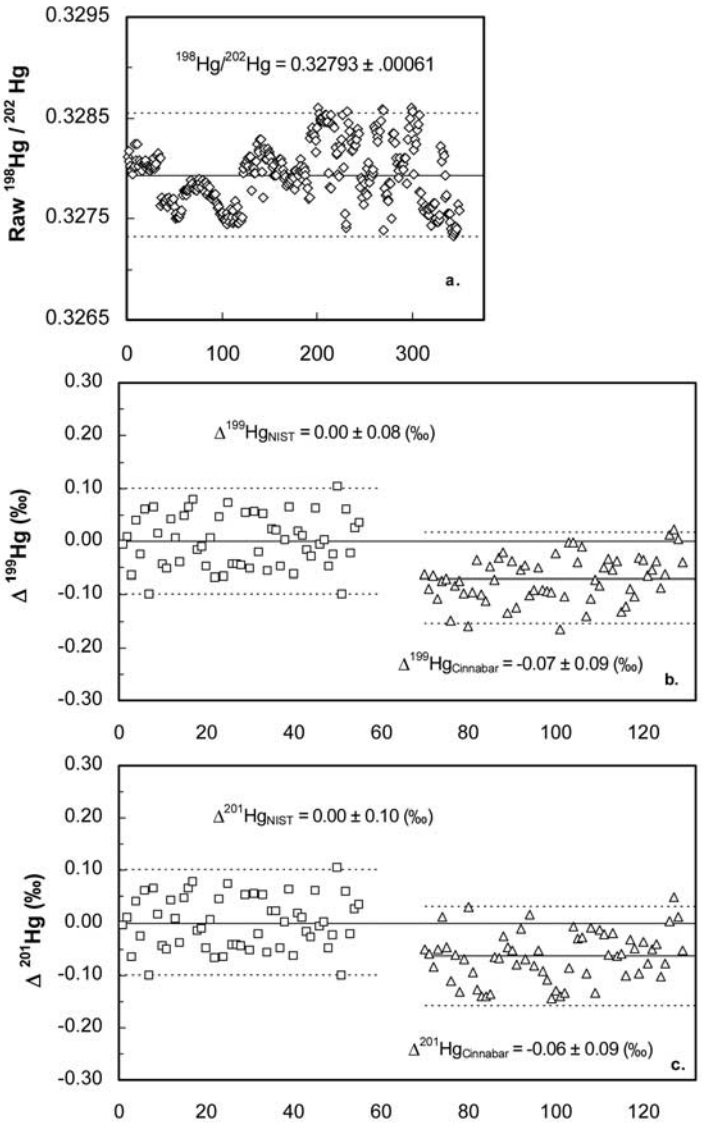

Figure 1. Long-term reproducibility for Hg isotope ratios determined at National High Magnetic Field Laboratory by multicollector inductively coupled plasma–mass spectrometry: (a) Raw $^{198}Hg/^{202}Hg$ calculated directly from signal intensities for 350 replicate measurements of NIST SRM 3133 Hg standard (1 ng mL^{-1}) collected over a time period of 6 months, (b) $\Delta^{199}Hg$ (‰) for 55 replicate measurements of Hg from NIST SRM 3133 (1 ng mL^{-1}) and 60 replicate measurements of Hg from Almaden cinnabar (1 ng mL^{-1}), representing 4 months of data collection, and (c) same as in Figure 1b for $\Delta^{201}Hg$ (‰). The bold lines represent the estimated average, and the dashed lines represent the $\pm 2\sigma$ uncertainty.

[*Hahn et al.*, 1979]. These values of A_{NV} (Table 4) were close to those obtained by *Schauble* [2007], with the notable exception of the scale factor for ^{204}Hg. The scale factors calculated from nuclear radii determined by *Hahn et al.* [1979] in Table 4 indicate that ^{204}Hg behaves in an entirely mass-dependent manner, consistent with fractionations observed in the natural samples. Mass-independent fractionations calculated from the revised A_{NV} values are shown in Figure 3a for each of the species for which $\delta^{198}Hg$ is available [*Schauble*, 2007]. It can be seen that equilibrium isotope effects that include the nuclear field shift give rise to a nonzero value of $\Delta^{199}Hg$ the magnitude of which is a function of the chemical species (Figure 3a), with reduced species (Hg^0, methylmercury) featuring positive anomalies. Further, the nuclear field shift effect is larger in $\Delta^{199}Hg$ than in $\Delta^{201}Hg$ by about a factor of two. For comparison, Figure 3b is a plot of the data from our analyses (Table 1).

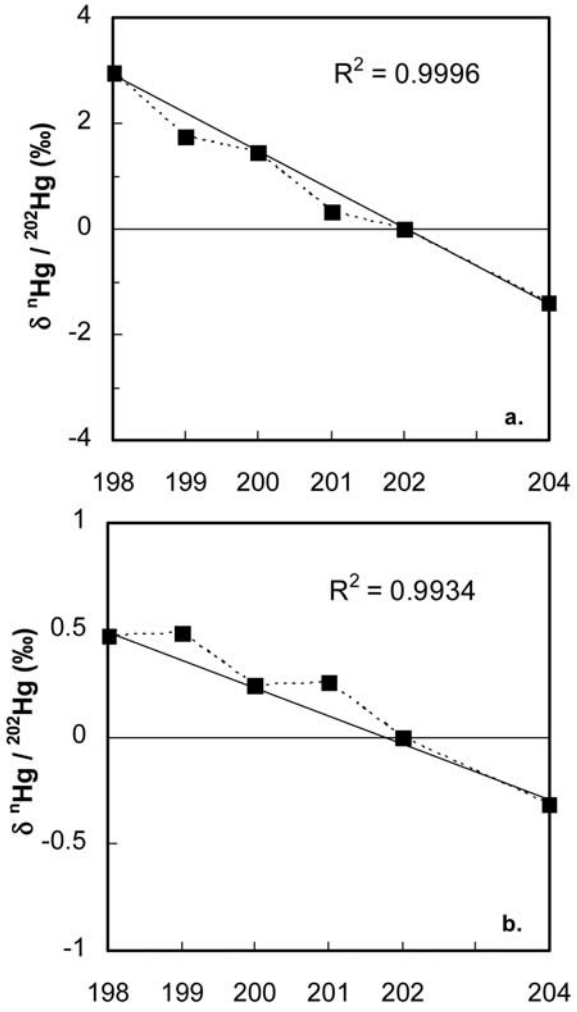

Figure 2. Selected δ $^{n}Hg/^{202}Hg$ (per mil) (where n = 198, 199, 200, 201, 202, and 204) value of (a) peat (58–60, peat core) and (b) sediment standard (NIST SRM 2710) as a function of mass number of mercury isotopes, illustrating the mass-independent fractionation observed in odd A isotopes of Hg. The measured isotopic ratio is converted to per mil deviation (δ notation) with respect to measurements of the NIST SRM3133 Hg standard performed by standard-sample bracketing. The black lines represent a linear regression through the even A isotopes of Hg, which show only mass-dependent fractionation.

[14] The magnetic isotope effect is a kinetic phenomenon and depends on reaction rates, reaction mechanisms involving radical pairs and their mean lives, and nuclear magnetic moments of reactant isotopes. This effect is observed in spin-selective reactions of paramagnetic particles and leads to fractionation into magnetic and nonmagnetic isotopes [*Buchachenko et al.*, 1976; *Turro*, 1983]. Only the odd A isotopes of mercury have nonzero nuclear spin quantum numbers (^{199}Hg and ^{201}Hg, have nuclear spins of 1/2 and 3/2 and magnetic moments +0.5029 and −0.5602 μ_B, respectively). Accordingly magnetic isotope effects can produce

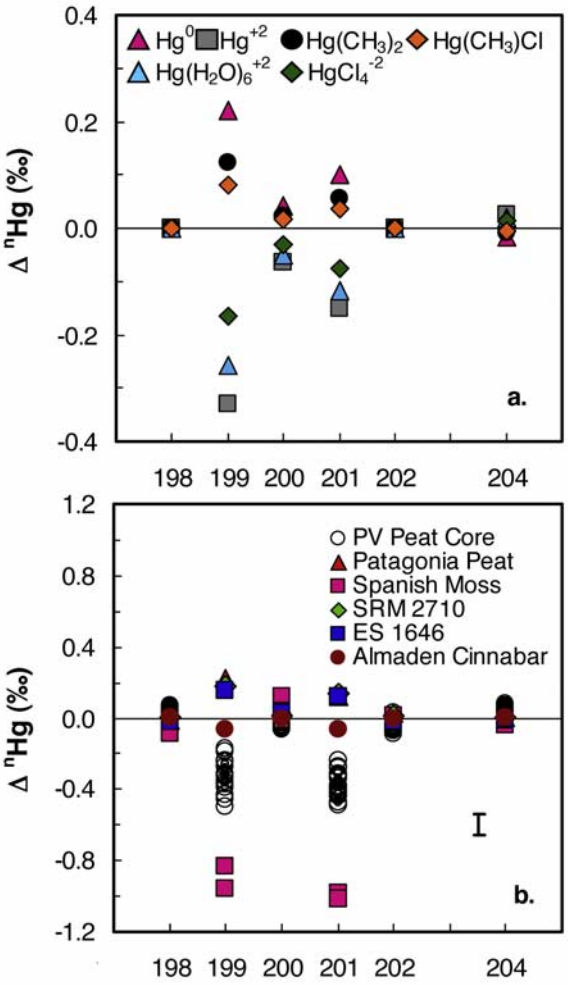

Figure 3. Nuclear field shift mass-independent fractionation, $\Delta^{n}Hg$ per mil as a function of mass number of mercury isotopes (see text for details). (a) Theoretical $\Delta^{n}Hg$ per mil (from equation (3)) for important oxidized and reduced mercury-bearing chemical species of environmental interest, normalized relative to fractionation factors for $HgCl_2$. The A_{NV} factors from Table 4 are calculated using RMS nuclear charge radii [*Hahn et al.*, 1979] values from muonic X-ray transitions. (b) Mass-independent fractionation, $\Delta^{n}Hg$ per mil, for Hg from natural samples (this study). Sediment standards ES1646 and SRM 2710 and Patagonia peat show positive mass-independent anomaly on the odd isotopes. The Penido Vello (PV) peat core (open circles) and Spanish moss show negative mass-independent anomaly on odd isotopes. The average of Almaden cinnabar determined from 60 replicate runs shows very little deviation from mass-dependent effect. A representative error bar is shown.

Table 4. Nuclear Volume Scale Factors Calculated From Nuclear Radii Determined by *Hahn et al.* [1979] and Δ^nHg Values Calculated for Various Mercury-Bearing Chemical Species Relative to $HgCl_2$[a]

	$^{198}Hg/^{202}Hg$	$^{199}Hg/^{202}Hg$	$^{200}Hg/^{202}Hg$	$^{201}Hg/^{202}Hg$	$^{202}Hg/^{202}Hg$	$^{204}Hg/^{202}Hg$
NV scale factor	1.0000	0.9200	0.5288	0.3256	0.0000	−0.4990
Chemical Species	Δ^{198}Hg	Δ^{199}Hg	Δ^{200}Hg	Δ^{201}Hg	Δ^{202}Hg	Δ^{204}Hg
Hg^0	0.00	0.22	0.04	0.10	0.00	−0.02
Hg^{+2}	0.00	−0.33	−0.06	−0.15	0.00	0.03
$Hg(CH_3)_2$	0.00	0.12	0.02	0.06	0.00	−0.01
$Hg(CH_3)Cl$	0.00	0.08	0.02	0.04	0.00	−0.01
$HgCl_2$	0.00	0.00	0.00	0.00	0.00	0.00
$HgBr_2$	0.00	0.01	0.00	0.00	0.00	0.00
$Hg(H_2O)_6^{+2}$	0.00	−0.26	−0.05	−0.12	0.00	0.02
$HgCl_4^{-2}$	0.00	−0.17	−0.03	−0.08	0.00	0.01

[a] All nuclear volume fractionation factors are calculated at 25°C. NV is nuclear volume.

a partial separation of ^{199}Hg and ^{201}Hg from each other and from the even A isotopes of mercury.

[15] Samples including Patagonia peat, various sediments, and cinnabar plot close to the theoretical nuclear field shift relationship between Δ^{199}Hg and Δ^{201}Hg (Figure 4). The Penido Vello peat and the Spanish moss samples notably exhibit a Δ^{199}Hg approximately equal to Δ^{201}Hg. Thus if Hg nuclear radii are accurately determined, this additional source of mass-independent fractionation likely is due to magnetic isotope effects. For reference, two lines, one with Δ^{201}Hg = 0.4569 * Δ^{199}Hg (as predicted by nuclear volume effect and recalculated in this work) and other Δ^{201}Hg = 1.11 * Δ^{199}Hg (where 1.11 is the ratio of the nuclear magnetic moments of ^{201}Hg to ^{199}Hg and the best estimate of the relative magnetic isotope effects) [*Buchachenko et al.*, 2004] fitted to go through the point (0.0, 0.0) are drawn on Figure 4. The third line (dashed) is the calculated nuclear volume fractionation line from *Schauble* [2007], which agrees well with the line calculated in this study, indicating that the RMS nuclear charge radii of *Hahn et al.* [1979] agree well with those of *Angeli* [2004] for the odd isotopes. When considered altogether, the samples roughly follow the magnetic isotope effect line with a slope of 1.11. Values of the Δ^{199}Hg/Δ^{201}Hg ratios range from 0.54 to 2.00 (Table 3).

[16] In Figure 4 lines defining the Δ^{201}Hg/Δ^{199}Hg ratios produced by the effects of magnetic spin and nuclear volume are drawn for comparison. From the isotopic data it appears to be possible to differentiate the relative contribution of nuclear volume effect and magnetic spin effect (Table 3). Assuming that the MIF anomalies are artifacts of only two different isotope effects, one producing Δ^{201}Hg/Δ^{199}Hg in a ratio of 0.4569 and the other in a ratio of 1.11 we have calculated the relative contributions of each effect to the total MIF. In the sediment standards the nuclear field shift effect and

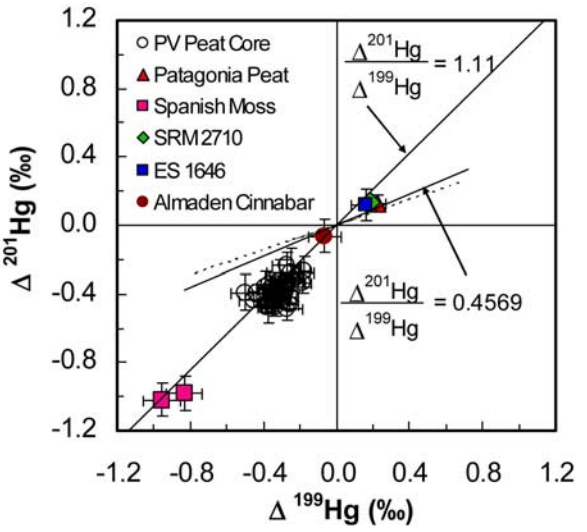

Figure 4. Calculated Δ^{199}Hg per mil versus Δ^{201}Hg per mil values in peat, sediments, moss, and cinnabar. The dotted line and short solid line define the expected covariation between Δ^{199}Hg and Δ^{201}Hg based on theoretical nuclear field shift from *Schauble* [2007] and recalculated in this work, respectively. The Δ^{201}Hg/Δ^{199}Hg = 1.11 line is predicted from magnetic moments of the two isotopes and drawn for reference to facilitate discussion. The internal precision of each measurement was calculated as the 2 SE of the mean of n runs, where n = 50, or multiples of 50 for larger samples. For Almaden cinnabar the error represents 2σ on 60 replicate measurements. Note that Hg from the Penido Vello peat and from the Spanish moss does not plot along the theoretical mass-independent line calculated from nuclear field shift alone.

magnetic isotope effect both seem to play an equivalent role in fractionating mass independently (Table 3 and Figure 4) and samples plot in between the two trend lines defined by the two different processes. The dominant process for the Patagonia peat seems to be the nuclear field shift effect. The dominant process for the Penido Vello peat core and Spanish moss is consistent with the magnetic isotope effect.

4. Conclusion

[17] Mass-independent fractionation has been an important tracer in light element geochemistry. Here we show it to be an equally important tracer for heavy element geochemistry of Hg. The nuclear field shift induces a mass-independent isotope effect in the odd A Hg isotopes in the ratio, $\Delta^{201}Hg/\Delta^{199}Hg \approx 0.5$, with the odd A isotopes concentrated in the reduced Hg species (Hg^0 and methylmercury). After substitution of empirically determined nuclear radii as inputs in calculating separation factors for Hg isotopes, no mass-independent effect on $\Delta^{204}Hg$ is predicted, and none is observed. The sediment samples and the Patagonia peat are enriched in the odd A Hg isotopes in approximately correct ratios for nuclear field shift effect, while the Penido Vello and Spanish moss samples are depleted in the odd A Hg isotopes. Because the Penido Vello peat core samples and the Spanish moss, both of which receive their Hg from the atmosphere, exhibit $\Delta^{201}Hg/\Delta^{199}Hg \approx 1$ an additional source of mass-independent isotope fractionation based on magnetic isotope effect is inferred. The potential for isotopic tracing of Hg speciation in the environment should have important implications for a better understanding of the behavior of mercury in the environment and eventually provide important constraints on models of the mercury cycle, including both natural and anthropogenic influences.

Acknowledgments

[18] These results sprouted from research supported by the U.S. EPA through STAR Grant R-83060301 and NSF award 0106789. Although the research described in this article has been funded in part by the United States Environmental Protection Agency through STAR Grant R-83060301 to A. L. Odom, V. Salters, and W. Landing, it has not been subjected to the agency's required peer and policy review and therefore does not necessarily reflect the views of the agency, and no official endorsement should be inferred. Discussions and advice from M. Bizimis, V. Salters, and W. Landing have helped us over a number of obstacles. Our initial analyses (Spanish moss) were performed at UC Santa Cruz, and for this we thank J. Aggarwal. A. Martinez-Cortizas graciously made it possible for C. Kinyon-Bingel and M. Gaboardi to collect the Penido Vello peat core. H. Beister kindly provided the Patagonia peat sample. We thank E. Schauble and an anonymous reviewer for improvements.

References

Angeli, I. (2004), A consistent set of nuclear rms charge radii: Properties of the radius surface R(N, Z), *At. Data Nucl. Data Tables*, *87*(2), 185–206.

Benoit, J. M., W. F. Fitzgerald, and A. W. H. Damman (1994), Historical atmospheric mercury deposition in the mid-Continental U.S. as recorded in an ombrotrophic peat bog, in *Mercury Pollution: Integration and Synthesis*, edited by C. J. Watras and J. W. Huckabee, pp. 187–202, Lewis, Boca Raton, Fla.

Bergquist, B. A., and J. D. Blum (2007), Mass-dependent and -independent fractionation of Hg isotopes by photoreduction in aquatic systems, *Science*, *318*(5849), 417–420.

Biester, H., G. Muller, and H. F. Scholer (2002), Binding and mobility of mercury in soils contaminated by emissions from chlor-alkali plants, *Sci. Total Environ.*, *284*(1–3), 191–203.

Biester, H., A. Martinez-Cortizas, S. Birkenstock, and R. Kilian (2003), Effect of peat decomposition and mass loss on historic mercury records in peat bogs from Patagonia, *Environ. Sci. Technol.*, *37*(1), 32–39.

Bigeleisen, J. (1996), Nuclear size and shape effects in chemical reactions: Isotope chemistry of the heavy elements, *J. Am. Chem. Soc.*, *118*(15), 3676–3680, doi:10.1021/ja954076k.

Bronsted, J. N., and G. Von Hevesy (1920), The separation of the isotopes of mercury, *Nature*, *106*, 144.

Buchachenko, A. L., E. M. Galimov, V. V. Ershov, G. A. Nikiforov, and A. D. Pershin (1976), Isotope enrichment induced by magnetic interactions in chemical reactions, *Dokl. Akad. Nauk SSSR*, *228*, 379–381.

Buchachenko, A. L., D. A. Kouznetsov, and A. V. Shishkov (2004), Spin biochemistry: Magnetic Isotope effect in the reaction of creatine kinase with CH_3HgCl, *J. Phys. Chem. A*, *108*(5), 707–710.

Buchachenko, A. L., V. L. Ivanov, V. A. Roznyatovskii, G. A. Artamkina, A. K. Vorob'ev, and Y. A. Ustynyuk (2007), Magnetic isotope effect for mercury nuclei in photolysis of bis(p-trifluoromethylbenzyl) mercury, *Dokl. Phys. Chem., Engl. Transl.*, *413*, 39–41.

Fitzgerald, W. F. (1995), Is mercury increasing in the atmosphere? The need for an atmospheric mercury network (AMNET), *Water Air Soil Pollut.*, *80*, 245–254.

Foucher, D., and H. Hintelmann (2006), High-precision measurement of mercury isotope ratios in sediments using cold-vapor generation multi-collector inductively coupled plasma mass spectrometry, *Anal. Bioanal. Chem.*, *384*(7), 1470–1478.

Gerstenkorn, S., and J. Verges (1975), Interpretation of the anomalous odd-even isotopes in the arc spectra of mercury, *J. Phys. Paris*, *36*, 481–486.

Grigal, D. F. (2003), Mercury sequestration in forests and peatlands: A review, *J. Environ. Qual.*, *32*(2), 393–405.

Hahn, A. A., J. P. Miller, R. J. Powers, A. Zehnder, A. M. Rushton, R. E. Welsh, A. R. Kunselman, P. Roberson, and H. K. Walter (1979), An experimental study of muonic x-ray transitions in mercury isotopes, *Nucl. Phys. A*, *314*, 361–386.

Hintelmann, H., and S. Lu (2003), High precision isotope ratio measurements of mercury isotopes in cinnabar ores using multi-collector inductively coupled plasma mass spectrometry, *Analyst*, *128*, 635–639.

Jackson, T. A., D. C. G. Muir, and W. F. Vincent (2004), Historical variations in the stable isotope composition of mercury in arctic lake sediments, *Environ. Sci. Technol.*, *38*(10), 2813–2821.

Klaue, B., and J. D. Blum (1999), Trace element analyses of arsenic in drinking water by inductively coupled plasma mass spectrometry: High resolution versus hydride generation, *Anal. Chem.*, *71*, 1408–1414.

Kritee, K., J. D. Blum, M. W. Johnson, B. A. Bergquist, and T. Barkay (2007), Mercury stable isotope fractionation during reduction of Hg(II) to Hg(0) by mercury resistant microorganisms, *Environ. Sci. Technol.*, *41*(6), 1889–1895.

Lindqvist, O., K. Johansson, M. Aastrup, A. Andersson, L. Bringmark, G. Hovsenius, L. Hakanson, A. Iverfeldt, M. Meili, and B. Timm (1991), Mercury in the Swedish environment—Recent research on causes, consequences and corrective methods, *Water Air Soil Pollut.*, *55*, xi–261.

Martínez-Cortizas, A., X. Pontevedra-Pombal, E. García-Rodeja, J. C. Nóvoa-Muñoz, and W. Shotyk (1999), Mercury in a Spanish peat bog: Archive of climate change and atmospheric metal deposition, *Science*, *284*(541), 939–942.

Mason, R. P., and G.-R. Sheu (2002), Role of the ocean in the global mercury cycle, *Global Biogeochem. Cycles*, *16*(4), 1093, doi:10.1029/2001GB001440.

Meili, M. (1991), The coupling of mercury and organic-matter in the biogeochemical cycle—Towards a mechanistic model for the boreal forest zone, *Water Air Soil Pollut.*, *56*, 333–347.

Mierle, G., and R. Ingram (1991), The role of humic substances in the mobilization of mercury from watersheds, *Water Air and Soil Pollution*, *56*, 349–357.

Morel, F. M. M., A. M. L. Kraepiel, and M. Amyot (1998), The chemical cycle and bioaccumulation of mercury, *Annu. Rev. Ecol. Syst.*, *29*(1), 543–566.

Nier, A. O. (1950), A redetermination of the relative abundances of the isotopes of neon, krypton, rubidium, xenon, and mercury, *Phys. Rev.*, *79*(3), 450–454.

Schauble, E. A. (2007), Role of nuclear volume in driving equilibrium stable isotope fractionation of mercury, thallium, and other very heavy elements, *Geochim. Cosmochim. Acta*, *71*(9), 2170–2189.

Schuster, E. (1991), The behavior of mercury in the soil with special emphasis on complexation and adsorption processes—A review of the literature, *Water Air Soil Pollut.*, *56*, 667–680.

Smith, C. N., S. E. Kesler, B. Klaue, and J. D. Blum (2005), Mercury isotope fractionation in fossil hydrothermal systems, *Geology*, *33*(10), 825–828.

Turro, N. J. (1983), Influence of nuclear spin on chemical, reactions: Magnetic isotope and magnetic field effects (a review), *Proc. Natl. Acad. Sci. U. S. A.*, *80*, 609–621.

Xia, K., U. L. Skyllberg, W. F. Bleam, P. R. Bloom, E. A. Nater, and P. A. Helmke (1999), X-ray absorption spectroscopic evidence for the complexation of Hg(II) by reduced sulfur in soil humic substances, *Environ. Sci. Technol.*, *33*(2), 257–261.

Yin, Y. J., H. E. Allen, C. P. Huang, D. L. Sparks, and P. F. Sanders (1997), Kinetics of mercury(II) adsorption and desorption on soil, *Environ. Sci. Technol.*, *31*(2), 496–503.